# Direct observation of conformational population shifts in crystalline human hemoglobin

Received for publication, March 7, 2017, and in revised form, August 15, 2017 Published, Papers in Press, September 20, 2017, DOI 10.1074/jbc.M117.781146

**Naoya Shibayama**[‡1], **Mio Ohki**[§], **Jeremy R. H. Tame**[§], **and Sam-Yong Park**[§]

*From the* [‡]*Department of Physiology, Division of Biophysics, Jichi Medical University, 3311-1 Yakushiji, Shimotsuke, Tochigi 329-0498 and the* [§]*Drug Design Laboratory, Graduate School of Medical Life Science, Yokohama City University, 1-7-29 Suehiro, Tsurumi, Yokohama 230-0045, Japan*

Edited by Wolfgang Peti

**Although X-ray crystallography is the most commonly used technique for studying the molecular structure of proteins, it is not generally able to monitor the dynamic changes or global domain motions that often underlie allostery. These motions often prevent crystal growth or reduce crystal order. We have recently discovered a crystal form of human hemoglobin that contains three protein molecules allowed to express a full range of quaternary structures, whereas maintaining strong X-ray diffraction. Here we use this crystal form to investigate the effects of two allosteric effectors, phosphate and bezafibrate, by tracking the structures and functions of the three hemoglobin molecules following the addition of each effector. The X-ray analysis shows that the addition of either phosphate or bezafibrate not only induces conformational changes in a direction from a relaxed-state to a tense-state, but also within relaxed-state populations. The microspectrophotometric $O_2$ equilibrium measurements on the crystals demonstrate that the binding of each effector energetically stabilizes the lowest affinity conformer more strongly than the intermediate affinity one, thereby reducing the $O_2$ affinity of tense-state populations, and that the addition of bezafibrate causes an ~5-fold decrease in the $O_2$ affinity of relaxed-state populations. These results show that the allosteric pathway of hemoglobin involves shifts of populations rather than a unidirectional conversion of one quaternary structure to another, and that minor conformers of hemoglobin may have a disproportionate effect on the overall $O_2$ affinity.**

Large-scale conformational changes are thought to underlie the biological functions of many proteins. Perhaps the best studied is the tense-state (T)[2] to relaxed-state (R) transition in human hemoglobin (Hb), an $(\alpha\beta)_2$ tetrameric oxygen transport protein in red blood cells (Fig. 1*a*). The textbook description is that of a large quaternary structural change, involving the relative movement of two $\alpha\beta$ dimers ($\alpha1\beta1$ and $\alpha2\beta2$) by about 14° of rotation, occurs upon ligand binding and is a response for the allosteric regulation of Hb (1–3).

However, it has become increasingly apparent that Hb exists in an ensemble of multiple quaternary conformations. This complexity was first realized when the crystal structure of a second relaxed-state, R2, was solved nearly 25 years ago (4). An important fact is that in the T to R2 transition the two $\alpha\beta$ dimers rotate relative to each other by about 10° beyond R, implying that R2 has a substantially different quaternary conformation from R (Fig. 1*a*). Subsequent crystallographic studies have revealed that a number of quaternary structures lying between R and R2 can be obtained under different crystallization conditions (5–7). NMR studies also show that the averaged structure of CO-liganded Hb in solution is a dynamic intermediate between the R and R2 crystal structures (8). In addition to the relaxed-state structures, several pieces of evidence obtained from functional and structural studies suggest the existence of multiple forms of the tense-state of human Hb (9–12). These findings are in agreement with the view that Hb is in motion, fluctuating among many conformations that include the crystallographically observed structures, T, R, and R2.

Although X-ray crystallography has provided atomic details of the structures of particular conformers of Hb, it does not give direct information about molecular motions between them, limiting the understanding of the pathway of the conformational transition. Also, no static structure can reveal an allosteric mechanism in which conformational ensembles shift in response to external influences.

Recently, we discovered a novel *C*2 crystal form of Hb, which not only contains three independent Hb tetramers with different structures, but also allows those molecules to adopt a variety of conformations, depending on the conditions (13). We have shown that $\alpha1\beta2$ CO-liganded, cross-linked Fe(II)-Ni(II) hybrid Hb (*i.e.* XL[$\alpha$(Fe-CO)$\beta$(Ni)][$\alpha$(Ni)$\beta$(Fe-CO)]) with and without 10 mM $P_i$ (referred to as $HL^+$ and $HL^-$, respectively) and uncross-linked fully water-liganded met-Hb with 10 mM $P_i$ all crystallize in this *C*2 form. The nine tetramer models in the three crystal structures cover the complete conformational space of Hb, spanning from T to R2 via R, with various inter-

This work was supported by Japan Society for the Promotion of Science (JSPS) KAKENHI Grants JP15H01646 (to N. S.) and JP16K07326 (to N. S.). The authors declare that they have no conflicts of interest with the contents of this article.

*The atomic coordinates and structure factors (codes 5X2R, 4X2U, 5X2T, and 5X2S) have been deposited in the Protein Data Bank (http://wwpdb.org/).*

[1] To whom correspondence should be addressed. Tel.: 81-285-58-7308; Fax: 81-285-40-6294; E-mail: shibayam@jichi.ac.jp.

[2] The abbreviations used are: T, tense-state; R, relaxed-state; Hb, hemoglobin; R2, a second relaxed-state; XL[$\alpha$(Fe-CO)$\beta$(Ni)][$\alpha$(Ni)$\beta$(Fe-CO)], $\alpha1\beta2$ CO-liganded, cross-linked Fe(II)-Ni(II) hybrid Hb, where XL denotes the presence of fumaryl cross-link between the two Lys$\beta$-82 residues; $HL^-$, XL[$\alpha$(Fe-CO)$\beta$(Ni)][$\alpha$(Ni)$\beta$(Fe-CO)] without anions; RR2, an intermediate between R and R2; TR, an intermediate between T and R; BZF, bezafibrate; IHP, inositol hexaphosphate; PDB, Protein Data Bank; r.m.s. deviation, root mean square deviation; PEG, polyethylene glycol; MWC, Monod-Wyman-Changeux; TTS, tertiary two-state.

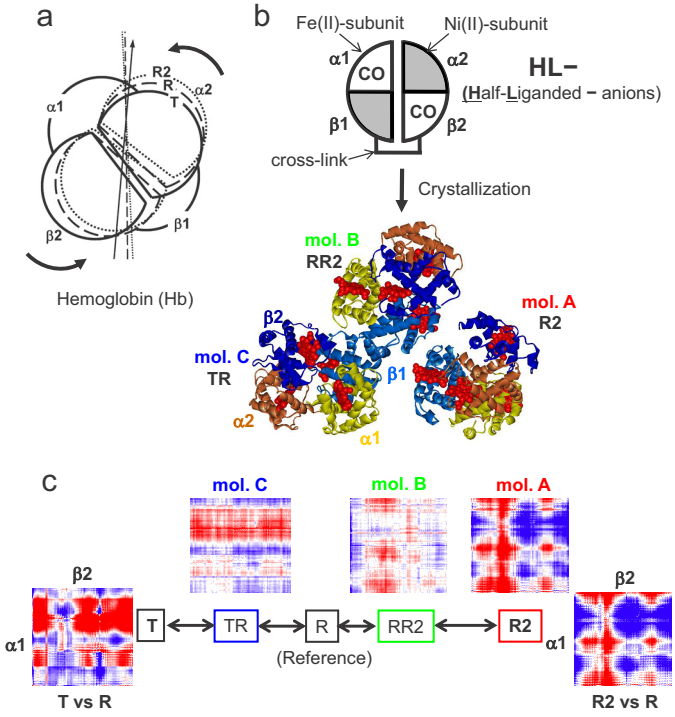


**Figure 1. Hb and its half-liganded model.** *a*, schematic showing the orientation of the $\alpha2\beta2$ dimers relative to the $\alpha1\beta1$ dimers in the T-, R-, and R2-states of Hb. The $\alpha1\beta1$ dimers are superposed. *b*, schematic of XL[$\alpha$(Fe-CO)$\beta$(Ni)][$\alpha$(Ni)$\beta$(Fe-CO)] without anions ($HL^-$; the starting sample) whose crystals contain three Hb molecules, A, B, and C (13). *c*, difference distance matrix plots of the $\alpha1\beta2$ subunits for molecules A, B, and C in the $HL^-$ crystal (PDB ID 4N7P) using R (PDB ID 2DN3) as a reference. *Red* indicates closer together than R and *blue* indicates the opposite. The color range extends from −1.5 Å (*dark blue*) to 1.5 Å (*dark red*).

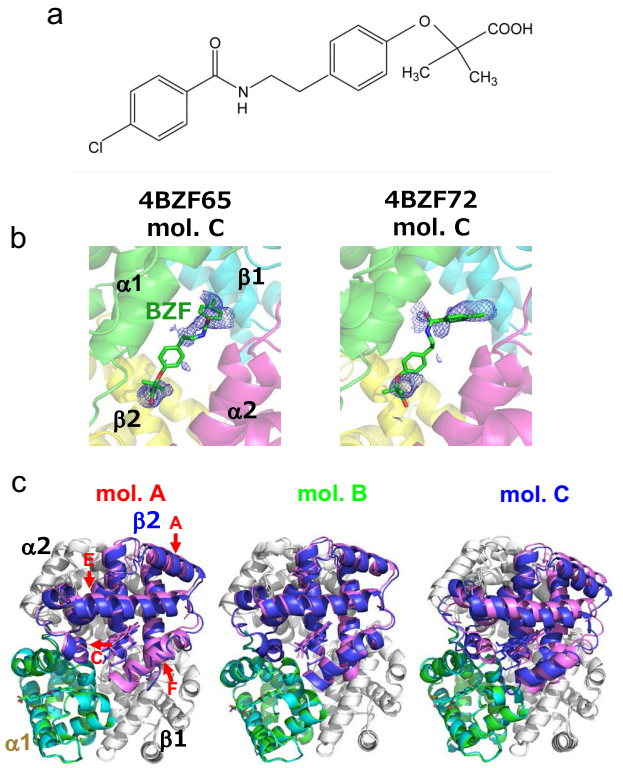


**Figure 2. An allosteric effector BZF and its binding to Hb.** *a*, chemical structure of BZF. *b*, electron density maps of the BZF molecules bound to the central water cavities of molecules C in 4BZF65 and 4BZF72. The $2F_o - F_c$ electron density maps contoured at 1.0$\sigma$ are shown as a *blue mesh*. For clarity, the BZF molecules are shown as a stick model. The mean *B*-values for the BZF molecules in 4BZF65 and 4BZF72 are 132.52 and 123.95, respectively. *c*, ribbon diagrams showing orientation changes in the $\alpha2\beta2$ dimers relative to the $\alpha1\beta1$ dimers upon adding 4 mM BZF at pH 6.5. The C$\alpha$ atoms of the $\alpha1\beta1$ dimers before ($HL^-$) and after the addition of BZF (4BZF65) are superimposed. The $\beta2$ subunits before and after the addition of BZF are shown in *magenta* and *blue*, respectively. *Red* indicates the directions of motions of the A, C, E, and F helices in the $\beta2$ subunits. The r.m.s. deviation values of the $\alpha2\beta2$ dimers and rigid body dimer rotation angles for the conformational changes in molecules A, B, and C are 0.413 Å/1.73°, 0.325 Å/1.03°, and 0.610 Å/8.89°, respectively.

mediate forms (13). Thus, the usage of this crystal form would give the unique opportunity to perform a crystallographic tracking of how Hb molecules in crystals undergoing structural and functional changes in response to environmental changes.

In this study, we chose $HL^-$ (see Fig. 1*b*) as the starting sample for the following reasons. First, in the $HL^-$ crystal the three tetramers, termed molecules A, B, and C, assume R2, RR2 (an intermediate between R and R2), and TR (an intermediate between T and R), respectively (13), that are expected to move toward a more tense conformation upon adding an allosteric effector (see Fig. 1, *b* and *c*). Second, in solution a half-liganded species may be in an equilibrium among energetically comparable, but structurally distinct conformers (14), so that an effector can modulate the composition of conformational ensembles. In addition, the cross-linked Fe(II)-Ni(II) hybrid Hb is a good and stable model for partially liganded Fe(II)-Hb, because Ni(II)-heme is an ideal surrogate for deoxy Fe(II)-heme (15, 16), and the $\beta$–$\beta$ fumaryl cross-link does not alter the structure and function of human Hb (17, 18). Using this model system, we visualize how the conformational ensembles of tetrameric Hb respond to the addition of allosteric effectors.

## Results and discussion

We investigated the effects of two allosteric effectors, $P_i$ and bezafibrate (BZF, see Fig. 2*a*), on the conformational ensembles of XL[$\alpha$(Fe-CO)$\beta$(Ni)][$\alpha$(Ni)$\beta$(Fe-CO)]. In this study, we did not investigate the effects of 2,3-bisphosphoglycerate or inositol hexaphosphate (IHP), because the binding site for these effectors is blocked by the fumaryl cross-link (17, 18). Before X-ray analysis, we need to know the kinetics of structural changes that occur in the crystals. Previous studies showed that upon the quaternary conformational change of the Fe(II)-Ni(II) hybrid, quite large spectrophotometric changes in the Ni(II) subunits can be detected in relationship to the change in the strength of the proximal Ni-His bond (15, 16); namely the light absorption peak at 558 nm (corresponding to four-coordinated Ni(II)-heme) is increased under the conditions that stabilize the T-state (Fig. 3, *a* and *b*). Taking this advantage, the kinetics can be determined by measuring the absorbance changes of the crystals following the addition of $P_i$ or BZF. As shown in Fig. 3, *c* and *d*, the time courses of the absorbance changes are dependent on the crystal thickness, indicating that the kinetics are limited by diffusion of solutes, at least in the case of the thick crystals. However, our diffusion simulation shows that this is not the case for the thin crystals in which the diffusion kinetics are much faster than the observed absorption change, suggesting that the kinetics are limited by conformational transition rates. It is likely that BZF binding requires a larger (slower)

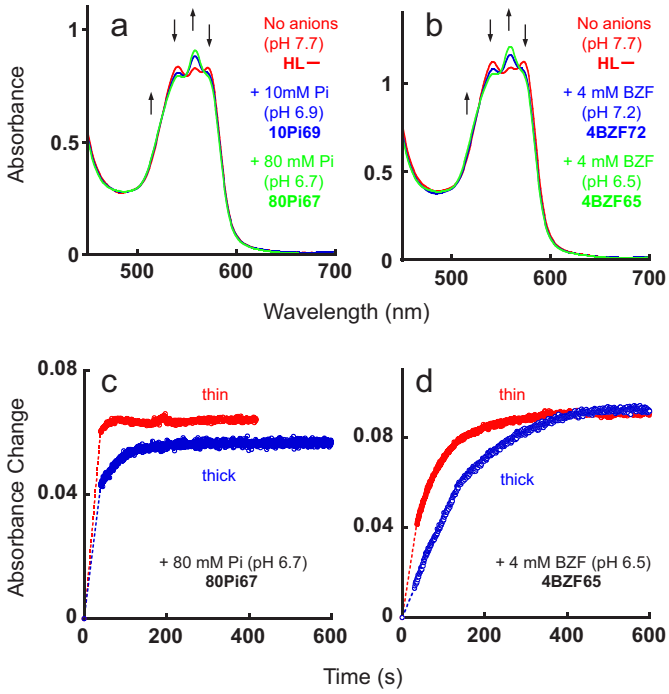


**Figure 3. Spectrophotometric monitoring of crystals upon the addition of either $P_i$ or BZF.** *a*, absorption spectra of a $HL^-$ crystal (*red line*; initial conditions without anions at pH 7.7) after a 14-min exposure to 10 mM $P_i$-K buffer (pH 6.9) (*blue line*), followed by a 16-min exposure to 80 mM $P_i$-K buffer (pH 6.7) (*green line*). *b*, absorption spectra of a $HL^-$ crystal (*red line*; initial conditions) after a 8-min exposure to 4 mM BZF and 20 mM HEPES buffer (pH 7.2) (*blue line*), followed by a 10-min exposure to 4 mM BZF and 20 mM MES buffer (pH 6.5) (*green line*). *c* and *d*, time courses of absorbance changes for thin (*red*) and thick (*blue*; 2.5–3.0 times thicker) crystals, observed at 558 and 516 nm, respectively, after transferring the $HL^-$ crystals to an 80 mM $P_i$-K buffer (pH 6.7) (shown in *c*) or to a 4 mM BZF and 20 mM MES buffer (pH 6.5) (shown in *d*).

conformational change to fit into its binding cavity than $P_i$, which binds more toward the surface.

Based on these data, the conformational ensembles under four sets of perturbed conditions examined in Fig. 3, *a* and *b*, were determined by X-ray crystallography after soaking intermediate-size $HL^-$ crystals (between those studied in Fig. 3, *c* and *d*) in each buffer for a sufficient time period. These crystals diffracted to better than a previously achieved 2.8-Å resolution for the original $HL^-$ crystal (13). The crystallographic parameters are summarized in Table 1. Electron density maps around the $\alpha1\beta2$ interfaces of all 12 conformers (3 tetramers × 4 conditions) illustrate the quality of the data collected (Fig. 4). Among them, we observed the weak electron density for BZF located at the central cavities of molecules C in 4BZF65 and 4BZF72 (Fig. 2*b*). In other tetramer models, there is little or no electron density for bound BZF or $P_i$. We note that, although the weak electron density and high temperature factors of the BZF molecule in our structural models (see Fig. 2*b*) do not permit us to define its occupancy precisely, the kinetics data in Fig. 3*d* ensure that the binding equilibrium is attained in the crystal. Perutz *et al.* (19) also noted in their X-ray study on the deoxy Hb–BZF complex that extension of the resolution beyond 2.5 Å did not improve the electron density map of BZF, because the high temperature factors of the BZF molecule were presumably associated with bond rotation. They found that the isobutyl group of BZF appears in the electron density map as a single unresolved sphere as we observed (see Fig. 2*b*), suggesting free rotation about the O–C bond.

Examples of quaternary conformational changes associated with effector binding are presented in Fig. 2*c*, including the structures of molecules A, B, and C before and after adding 4 mM BZF at pH 6.5. We should note that the resolutions of the current crystal structures (2.4–2.7-Å resolution) are high enough to discuss the quaternary states of the conformers (Fig. 4), but not high enough to allow for model construction of the CO molecules on the basis of the electron density maps. Moreover, as noted in our previous study (13), crystal lattices appear not to discriminate between two inequivalent dimers within the asymmetric tetramer (*i.e.* $\alpha1$(Fe-CO)$\beta1$(Ni) and $\alpha2$(Ni)$\beta2$(Fe-CO)). For these reasons, we do not model the CO molecules in the present structural models. The heme environmental structures cannot be discussed in detail either.

Conformational population shifts in response to adding $P_i$ or BZF are quantified by difference distance matrix plots that depict the changes in pairwise distances between all C$\alpha$ atoms, with respect to the initial structures (without anions) as a function of solution conditions (Fig. 5*a*). Significantly, during the solution changes, most conformers have experienced structural rearrangements at the quaternary level, as evidenced by the colors in the inter-dimer regions in Fig. 5*a*. The quaternary states of the 12 conformers can also be characterized based on the relative orientation of the two $\alpha\beta$ dimers (Fig. 1*a*), which is quantified by dimer–dimer rotation angle and rotation translation from T (Fig. 5, *b* and *c*).

To relate the obtained crystal structures to their $O_2$ affinities, we carried out $O_2$ equilibrium measurements on the single crystals under the same conditions as used for X-ray studies except for the absence of glycerol. The crystals were first converted to the oxy form and then equilibrated with different $O_2$ pressures. The optical absorption spectra of the crystals were measured by microspectrophotometry with light incident on the (010) crystal face. The fractional saturation of the ferrous hemes with $O_2$ ($Y$) was calculated by a least squares fit of the spectra to a linear combination of the reference spectra of the oxy-, deoxy-, and met-forms of the same crystal (Fig. 6).

The Hill plots of the $O_2$ equilibrium curves of the 10Pi69 (the final structural model of our *C*2 crystal after adding 10 mM $P_i$-K buffer, pH 6.9), 80Pi67 (the final structural model of our *C*2 crystal after adding 80 mM $P_i$-K buffer, pH 6.7), 4BZF72 (the final structural model of our *C*2 crystal after adding 4 mM BZF and 20 mM HEPES buffer, pH 7.2), and 4BZF65 (the final structural model of our *C*2 crystal after adding 4 mM BZF and 20 mM MES buffer, pH 6.5) crystals are shown in Fig. 7*a*, which for comparison includes the $O_2$ equilibrium curve of the initial $HL^-$ crystal without effector (13). As demonstrated in Fig. 7*b*, all the deoxygenation data obtained by the decreasing $O_2$ pressure (*open circles*) agree well with the oxygenation data obtained by increasing the $O_2$ pressure (*closed squares*), confirming that true equilibrium binding curves were being measured. Also, because the $HL^+$ crystal is a crystal grown under the conditions similar to the perturbed conditions of 10Pi69 (13), the agreement between the $O_2$ equilibrium curves of the 10Pi69 and $HL^+$ crystals ensures that a conformational equilibrium is reached in the crystal (Fig. 7*a*, *inset*).

**Table 1**
**Crystal parameters, data collection, and structure refinement**

| Data set | +10 mM $P_i$ (pH 6.9) | +80 mM $P_i$ (pH 6.7) | +4 mM BZF (pH 7.2) | +4 mM BZF (pH 6.5) |
|---|---|---|---|---|
| | **10Pi69** | **80Pi67** | **4BZF72** | **4BZF65** |
| **Data collection statistics** | | | | |
| Resolution range (Å) | 50.0–2.7 | 50.0–2.53 | 50.0–2.65 | 50.0–2.4 |
| Space group | *C*2 | *C*2 | *C*2 | *C*2 |
| Unit cell dimensions (Å) | $a = 228.77$, $b = 55.02$, $c = 138.43$, $\beta = 103.28°$ | $a = 228.89$, $b = 55.81$, $c = 139.93$, $\beta = 102.39°$ | $a = 228.49$, $b = 55.02$, $c = 138.50$, $\beta = 103.34°$ | $a = 228.60$, $b = 54.60$, $c = 138.44$, $\beta = 103.18°$ |
| Reflections (measured/unique) | 195,617/44,657 | 264,161/57,084 | 221,033/48,972 | 305,141/65,188 |
| Completeness (%) | 96.5 (83.5)[a] | 98.4 (87.6)[a] | 98.1 (83.9)[a] | 98.5 (97.4)[a] |
| Mean $\langle I\rangle/\langle\sigma(I)\rangle$ | 12.0 | 15.3 | 11.6 | 12.1 |
| multiplicity | 4.4 (3.8)[a] | 4.6 (4.1)[a] | 4.5 (3.4)[a] | 4.7 (4.6)[a] |
| $R_{merge}$ (%)[b] | 7.7 (48.0)[a] | 7.5 (37.9)[a] | 5.4 (58.1)[a] | 5.4 (58.2)[a] |
| *B*-factor from Wilson plot (Å$^2$) | 78 | 59 | 69 | 61 |
| **Refinement statistics** | | | | |
| Resolution range (Å) | 44.9–2.7 | 39.7–2.53 | 48.7–2.65 | 35.0–2.4 |
| *R*-factor (%)[c]/free *R*-factor (%) | 26.6/30.6 | 23.1/27.4 | 23.2/27.7 | 24.5/28.8 |
| R.m.s. deviations from ideals | | | | |
| Bond lengths (Å)/ bond angles (°) | 0.008/1.0 | 0.010/1.04 | 0.010/1.09 | 0.010/1.09 |
| *B*-values (all atoms) | | | | |
| Overall/mol-A/mol-B/mol-C | 80/81/76/83 | 68/64/63/78 | 76/78/76/76 | 79/86/77/73 |
| Ramachandran plot from MolProbity | | | | |
| Residues in most favorable regions (%) | 95.4 | 96.7 | 95.5 | 93.7 |
| Residues in allowed regions (%) | 4.1 | 3.2 | 4.0 | 5.5 |
| Residues in outlier regions (%) | 0.5 | 0.1 | 0.5 | 0.8 |
| Overall score | 2.18 | 1.74 | 2.16 | 2.33 |
| **PDB code** | 5X2R | 5X2U | 5X2T | 5X2S |

[a] Values in parentheses for the highest shell with a resolution of 2.75–2.70, 2.59–2.53, 2.70–2.65, and, 2.44–2.40 Å, respectively, from left to right.
[b] $R_{merge} = \Sigma|I_i - \langle I\rangle|/\Sigma|I_i|$, where $I_i$ is the intensity of an observation and $\langle I\rangle$ in the mean value for that reflection and the summations are over all reflections.
[c] *R*-factor $= \Sigma_h||F_o(h)| - |F_c(h)||/\Sigma_h F_o(h)$, where $F_o$ and $F_c$ are the observed and calculated structure factor amplitudes, respectively. Free *R*-factor was calculated with 5% of the data excluded from refinement.

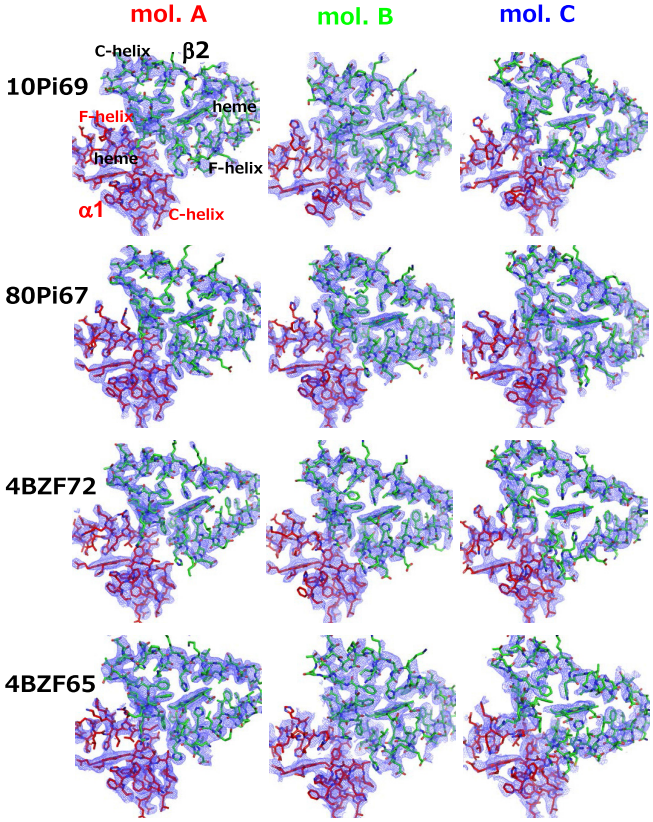


**Figure 4. Electron density maps around the $\alpha1\beta2$ interfaces of all the crystal structures solved in this study.** The $2F_o - F_c$ electron density maps contoured at 1.0$\sigma$ are shown as a *blue mesh*. The residues in the $\alpha1$ and $\beta2$ subunits are shown as *red* and *green sticks*, respectively.

We find that all the current crystals exhibit a biphasic curve with two distinct affinity components: one shows a sample-independent very low-affinity with no cooperativity (the right half of the Hill plot), and the other shows a sample-dependent high-affinity and a varied degree of cooperativity (the left half of the Hill plot). According to the previous assignment made on a similar biphasic curve of the $HL^+$ crystal (see Fig. 7*a*, *inset*), we can reasonably assign the low-affinity component as arising from molecule C, and the high-affinity component from molecules A and B.

Because the current crystals contain three independent hybrid Hb tetramers (see Fig. 1*b*), each with the $O_2$ binding equilibrium constants of the first and second oxygenation steps (*i.e.* $K_1$ and $K_2$), the number of parameters is too large to be evaluated with confidence from the experimental data. Thus, we must make some assumptions to limit their number. The first assumption is that $K_1$ and $K_2$ of molecules C (referred to as $K_{1C}$ and $K_{2C}$) in all the current crystals are the same as those of the $HL^+$ crystal previously determined (13). This assumption is reasonable for the following reasons. (i) As shown in Fig. 7*a*, all the current crystals show a similar low-affinity component (the right half of the Hill plot), which agrees well with that of the $HL^+$ crystal (Fig. 7*a*, inset), (ii) molecules C in the $HL^+$ and current crystals all adopt a similar T structure (Fig. 5), and (iii) it is shown that allosteric effectors (*e.g.* $H^+$, $Cl^-$, IHP, and BZF) do not alter the $O_2$ affinity of T-state Hb crystals (20–22). Then we assume that the remaining part of the data (the high-affinity component corresponding to molecules A and B) can be approximated by a simple two-step oxygenation scheme represented by the $O_2$ binding constants $K_{1AB}$ and $K_{2AB}$. Although this assumption is too simple to discriminate molecules A and B, in practice the $K_{2AB}$ value gives a good approximation to the overall $O_2$ affinity of relaxed-state populations. According to this biphasic model, all the curves could be well fitted (*solid lines* in Fig. 7) and the determined $O_2$ affinities listed in Table 2.

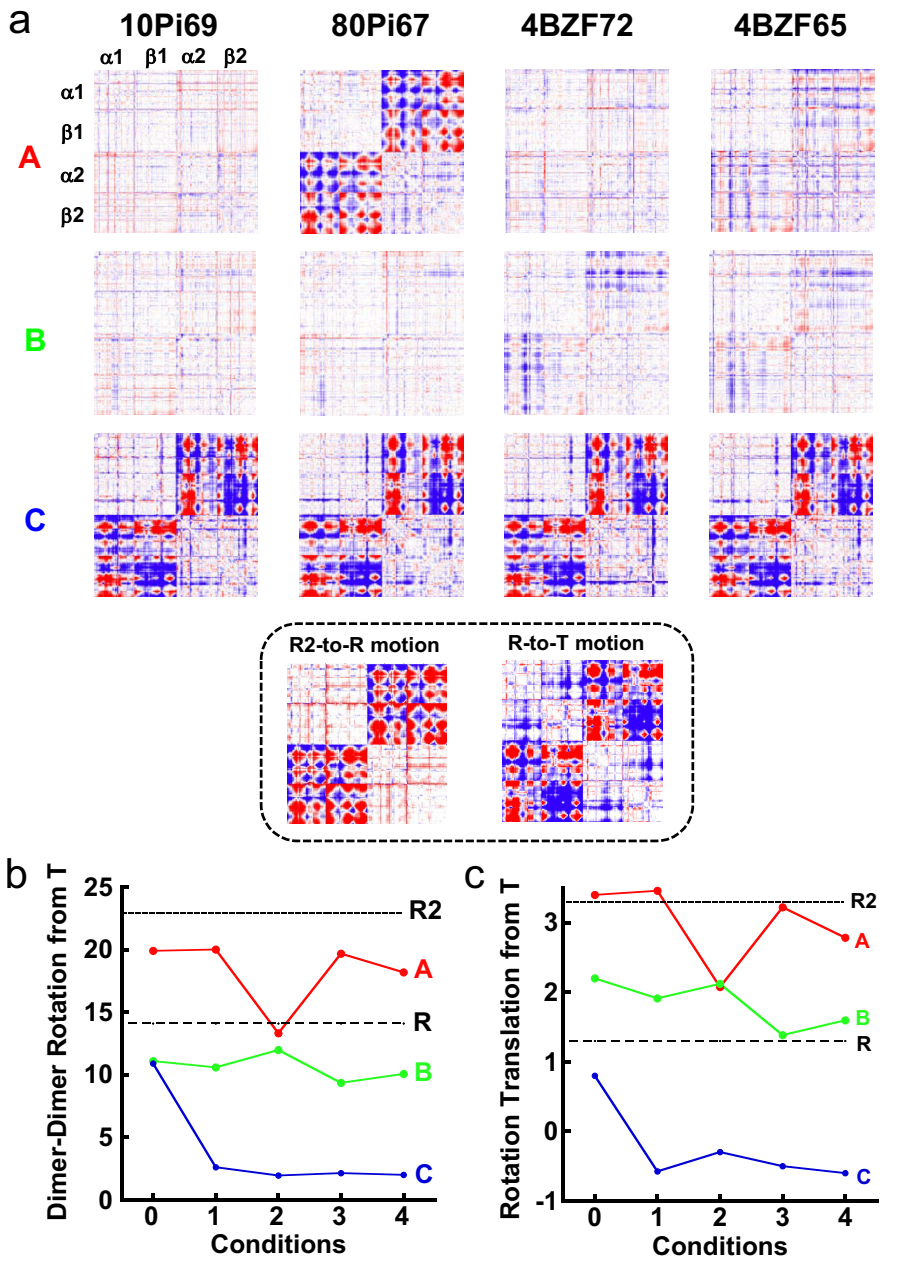


**Figure 5. Conformational population shifts in XL[$\alpha$(Fe-CO)$\beta$(Ni)][$\alpha$(Ni)$\beta$(Fe-CO)] in response to adding $P_i$ or BZF.** *a*, difference distance matrices of the ($\alpha1\beta1$)($\alpha2\beta2$) subunits for molecules A, B, and C in the $HL^-$ crystals upon the addition of $P_i$ or BZF. The initial structures with no anions (PDB ID 4N7P) are used as reference. *Red* indicates closer than the initial $HL^-$ and *blue* indicates the opposite. The color range extends from −1.5 Å (*dark blue*) to 1.5 Å (*dark red*). For comparison, the matrices representing the R2 to R and R to T motions are shown in the *dotted* area. *b*, dimer–dimer rotation angle (in degrees) from T (PDB ID 2DN2). Conditions 0, 1, 2, 3, and 4 correspond to $HL^-$ (initial), 10Pi69, 80Pi67, 4BZF72, and 4BZF65, respectively. *c*, rotation translation (in Å) from T. Note that the negative values for molecule C indicate the opposite direction to the values for R and R2. Conditions are the same as in *panel b*.

An interesting finding is that the addition of BZF decreases the $O_2$ affinity of relaxed-state populations by ~5-fold. Another finding worth mentioning is that the high-affinity components in the current crystals, except for 80Pi67, show a Hill coefficient smaller than unity (Table 2), indicating a slight (2–3-fold) functional difference between the $\alpha$ and $\beta$ subunits or between molecules A and B. Although we do not know why only the 80Pi67 crystal exhibits positive cooperativity in binding of $O_2$ (Table 2), it suggests that reversible ligand-linked conformational changes are allowed to occur in the 80Pi67 crystal.

We note here that $O_2$ equilibrium measurements on crystals require a high level of care and control, especially at low $O_2$ pressures in the presence of effector. Under these conditions, if the crystal quality is not sufficient and/or glycerol is present, $O_2$ binding is no longer reversible, which we tentatively interpret as being due to an irreversible conversion of a high-affinity conformer to a low-affinity one upon deoxygenation. If, however, the crystal quality is sufficient and glycerol is absent, crystals exhibit reversible $O_2$ binding at least in the range studied here (Fig. 7*b*).

A remarkable feature common to all the conditions studied is that molecule C exhibits a large amplitude conformational change from TR to a state that resembles the classical T (Fig. 5), indicating that in the presence of $P_i$ or BZF at acidic or neutral

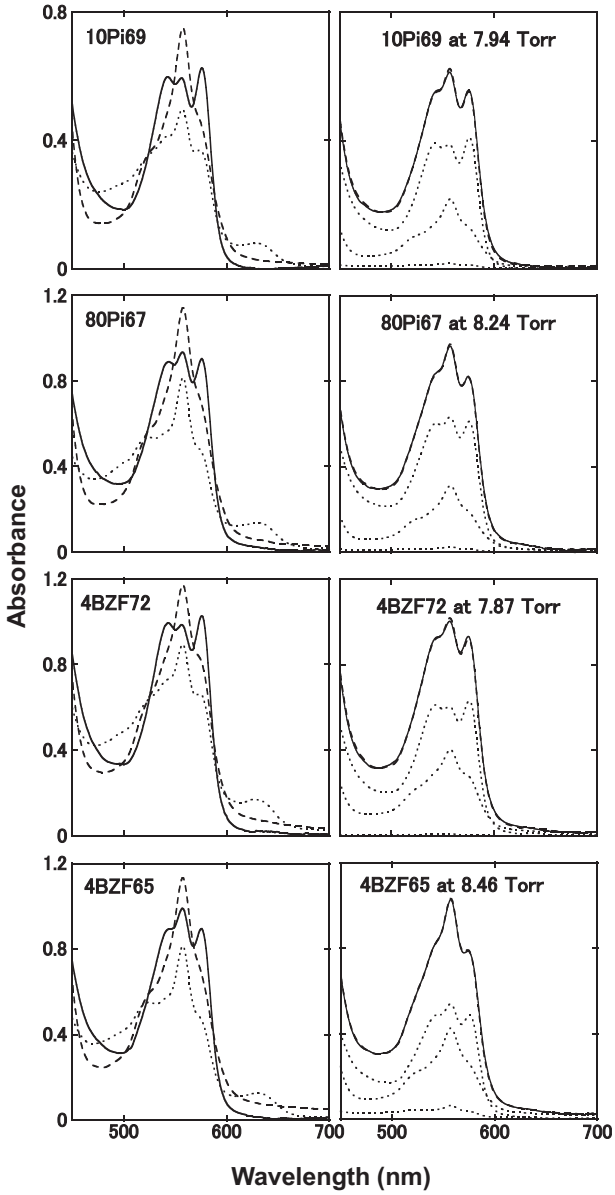


**Figure 6. Determination of the fractional saturation with $O_2$ of the ferrous hemes (*Y*) in the 10Pi69, 80Pi67, 4BZF72, and 4BZF65 crystals.** Panels on the *left* depict reference absorption spectra of the crystals. The spectra of the oxy-, deoxy-, and met-forms are shown as *solid*, *dashed*, and *dotted curves*, respectively. Panels on the *right* show examples of the fitting at an $O_2$ pressure of about 8 torr. *Y* was calculated by a least-square fit of the observed spectrum to a linear combination of corresponding three reference spectra and a baseline offset. In the *right panels*, the *solid curves* are the observed spectra, the *dashed curves* are the sums of the component reference spectra, and the *dotted curves* are the component reference spectra. The fractional amounts of oxy-, deoxy-, and met-forms are calculated to be 66.8, 29.7, and 3.5%, respectively, for the 10Pi69 crystal, 68.8, 27.8, and 3.4%, respectively, for the 80Pi67 crystal, 63.4, 35.5, and 1.1%, respectively, for the 4BZF72 crystal, and 54.5, 37.6, and 7.9%, respectively, for the 4BZF65 crystal.

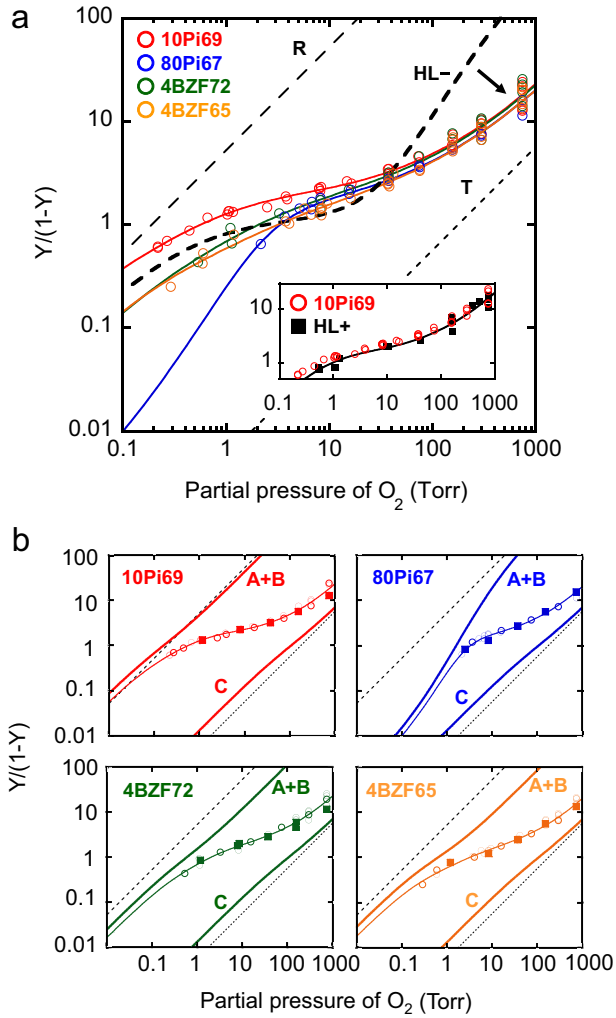


**Figure 7. $O_2$ equilibrium data for the 10Pi69, 80Pi67, 4BZF72, and 4BZF65 crystals.** *a*, Hill plots of $O_2$ dissociation curves for the crystals of 10Pi69 (*red*), 80Pi67 (*blue*), 4BZF72 (*green*), and 4BZF65 (*orange*). The *colored solid curves* through data points represent the least-squares fits with the biphasic model. The *bold dashed black curve* represents the $O_2$ equilibrium curve of the initial $HL^-$ crystal (13). The *dashed* and *dotted lines* represent the highest and lowest $O_2$ affinities of solution Hb, respectively (56). *Inset* shows the comparison of $O_2$ dissociation data of 10Pi69 (*red open circles*) and $HL^+$ (*black closed squares*). The *black solid curve* in the *inset* is the result of a least-squares to the data on $HL^+$. *b*, Hill plots that show reversibility and two affinity components in each crystal. The $O_2$ dissociation data (*open circles*) agree well with the corresponding association data (*filled squares*). The colored curves labeled as *A*+*B* and *C* represent the simulated curves for the sum of molecules A and B (high-affinity component), and those for molecule C (low-affinity component), respectively.

pH, T is energetically more favorable than TR within tense-state populations. Our recent $O_2$ equilibrium measurements on the *C*2 crystals show that TR exhibits an intermediate $O_2$ affinity (0.16 ± 0.09 $torr^{-1}$) between the affinities of T and R (*i.e.* 0.0064 ± 0.0020 $torr^{-1}$ and 3.8 ± 1.3 $torr^{-1}$, respectively) (13). The current $O_2$ equilibrium data provide direct evidence that the effector-induced conformational transition of TR to T is accompanied by a dramatic change in $O_2$ affinity (Fig. 7*a*).

These structural and functional results in crystals are in line with earlier solution studies, which show that the binding of anions to deoxy-Hb is linked to a conformational change from a TR-like intermediate-affinity state to a T-like low-affinity state (9, 11, 12), giving rise to a wide variation in the $O_2$ affinity of tense-state populations (23).

Another significant quaternary motion is seen in molecule A, which initially in the R2 form, shows a large R2 to R motion upon the addition of 80 mM $P_i$ buffer (pH 6.7) (Fig. 5). Similar motions, although smaller in magnitude, are seen in molecule A under the other three sets of conditions (Fig. 5). These findings indicate that anions (or salts) stabilize R relative to R2 within relaxed-state populations, which explains the fact that the R

**Table 2**
**$O_2$ affinity and cooperativity of crystals**

| Conditions | Molecules | $O_2$ affinity ($K_{2AB}$ or $K_{2C}$) | Cooperativity, Hill coefficient |
|---|---|---|---|
| | | *Torr*$^{-1}$ | *n* |
| 10Pi69: +10 mM $P_i$ (pH 6.9) | A+B | 4.2 ± 0.5 | 0.81 ± 0.08 |
| | C | 0.00646[a] | 0.82[a] |
| 80Pi67: +80 mM $P_i$ (pH 6.7) | A+B | 3.4 ± 2.7 | 1.7 ± 0.3 |
| | C | 0.00646[a] | 0.82[a] |
| 4BZF72: +4 mM BZF (pH 7.2) | A+B | 1.1 ± 0.4 | 0.80 ± 0.19 |
| | C | 0.00646[a] | 0.82[a] |
| 4BZF65: +4 mM BZF (pH 6.5) | A+B | 0.84 ± 0.17 | 0.70 ± 0.10 |
| | C | 0.00646[a] | 0.82[a] |
| HL−: no anions (pH 7.7)[b] | A+B | 5.2 ± 0.6 | 1.0[c] |
| | C | 0.16 ± 0.09 | 1.7 ± 0.2 |

[a] In the current analytical model, the $K_{1C}$ and $K_{2C}$ values of molecules C in the presence of effector are fixed to be 0.0132 torr$^{-1}$ and 0.00646 torr$^{-1}$, respectively (see text).
[b] Data from Shibayama *et al.* (13).
[c] In the previous study (13), it was assumed that molecules A and B show a similar high affinity without cooperativity ($n = 1$), then the $K_{1C}$ and $K_{2C}$ values of molecules C were determined by a least-squares fit (13).

crystal form has been traditionally grown under high-salt conditions such as high concentrations of phosphate or ammonium sulfate (2, 24–26), and the R2 form grown under low-salt conditions such as PEG (4, 27, 28), despite a few exceptions.

With regard to molecule B some quaternary motions can be detected, but their amplitudes are relatively small compared with molecules A and C (Fig. 5). This observation is again consistent with the stabilization of R by anions, as the initial conformation of molecule B (in the $HL^-$ crystal) lies closer to R than to R2 (with r.m.s. deviation of 0.77 Å over all 570 C$\alpha$ atoms when compared with R and 1.57 Å when compared with R2), corresponding to a structure near a free energy minimum regardless of the absence or presence of anions. We speculate that crystal packing around the B tetramer may favor R over the R2 and T conformations.

In contrast to the affinity variation in tense-state populations, the $O_2$ affinity of relaxed-state populations (corresponding to molecules A and B) is only modestly affected by the addition of effector (Table 2). The most significant effect is seen in 4BZF72 and 4BZF65, where a 5-fold decrease in affinity was observed as a result of the addition of BZF. However, within the resolution of our structural data, we are not able to determine how the binding of BZF affects the $O_2$ affinity of Hb.

To investigate further the dynamics of Hb molecules in crystals, we analyzed the crystallographic temperature factors (*i.e.* *B*-factors) of the main chain backbone atoms (Fig. 8). Because the *B*-values are linearly related to the mean square displacement of the atoms relative to their average positions (29), the comparison of *B*-values provides an interesting insight into the relative stability of three conformations in the same crystal (Fig. 8, *inset*). We find that as a whole, the *B*-value distributions depend significantly on the solution conditions and molecules (Fig. 8). More specifically, for example, although molecule C assumes a similar T conformation in all four conditions, it has the lowest *B*-value in 4BZF65, whereas the highest in 10Pi69 and 80Pi67 (Fig. 8, *inset*), suggesting that BZF is a stronger stabilizer for the T-state than $P_i$, especially at low pH. Previous X-ray analysis showed that BZF binds specifically to T-state deoxy-Hb at the central water cavity by contact with one $\beta$ and two $\alpha$ subunits to stabilize the T-state interface (19). By contrast, previous solution studies indicated that BZF binds only weakly and nonspecifically to CO-bound human Hb (19, 30), which may be in an ensemble of relaxed conformations (8). Consequently, it is likely that preferential binding of BZF at the T-state central cavity leads to additional stabilization of T relative to relaxed-state populations. This is confirmed by the electron density of BZF bound to the central cavities of T-state molecules C in 4BZF65 and 4BZF72 (Fig. 2*b*) and by its absence from molecules A and B, as described above. Also, this agrees with the B-factor distribution analysis, showing that the dimer–dimer contacts of molecules C in 4BZF65 and 4BZF72 are stabilized compared with those in 10Pi69 and 80Pi67 (Fig. 8).

Another notable feature in the *B*-value distributions is that, in 80Pi67, molecules A and B show a significantly smaller average value than that of molecule C (Fig. 8, *inset*). This can be explained as a consequence of the stabilization of R by anions as discussed above, because in 80Pi67, both molecules A and B are in a similar conformation close to R (Fig. 5) and is stabilized by $P_i$. We note that coexistence of the T- and R-states in 80Pi67 is consistent with earlier observations that under comparable conditions (*i.e.* in 100 mM $P_i$-K buffer, pH 7.0, at 20 °C) two other types of half-liganded Hbs (*i.e.* $\alpha1\alpha2$- and $\beta1\beta2$-liganded Hbs) also exist in a conformational ensemble of the 35–45% low-affinity state and 55–65% high-affinity state (14).

An additional interesting finding is that the asymmetric unit surface regions of the R2-like molecules (*e.g.* molecules A in 10Pi69, 4BZF72, 4BZF65, and $HL^-$) are destabilized by the addition of anions (Fig. 8). This may be related to the fact that the R2 crystal form has been traditionally grown under low-salt conditions (4, 27, 28).

In this work, effector-induced structural and functional changes in human Hb were observed directly by a combination of X-ray analysis and $O_2$ equilibrium measurements on a novel crystal form, which contains three distinct Hb tetramers in the asymmetric unit and also allows the global conformational switching of those molecules (Fig. 5). Unlike classical X-ray crystallography that usually determines only a single protein conformation under a given condition, our approach is able to track how Hb molecules in crystals undergo structural and functional changes depending on solution conditions. We show that conformational population shifts do indeed occur in human Hb in response to heterotropic ligands. We also show that effector-induced conformational population shifts are indeed accompanied by functional changes. Our results favor the Monod-Wyman-Changeux (MWC)-like pre-existing equilibrium model (1) over the Koshland-Nemethy-Filmer-like sequential model (31). We should emphasize that a conformational population shift is the basic concept of the original MWC model (1), as it postulates that Hb and other allosteric proteins exist in equilibrium between two (at least two) conformational states and the ensemble undergoes a population shift following the binding of ligand or allosteric effector. This concept has recently been extended and applied to a variety of biomolecular processes including protein–protein, protein–nucleic acid, and monomeric protein–ligand interactions (32, 33). Our results add new insight into the conformational population shifts in human Hb beyond the simple two-state conformational model.

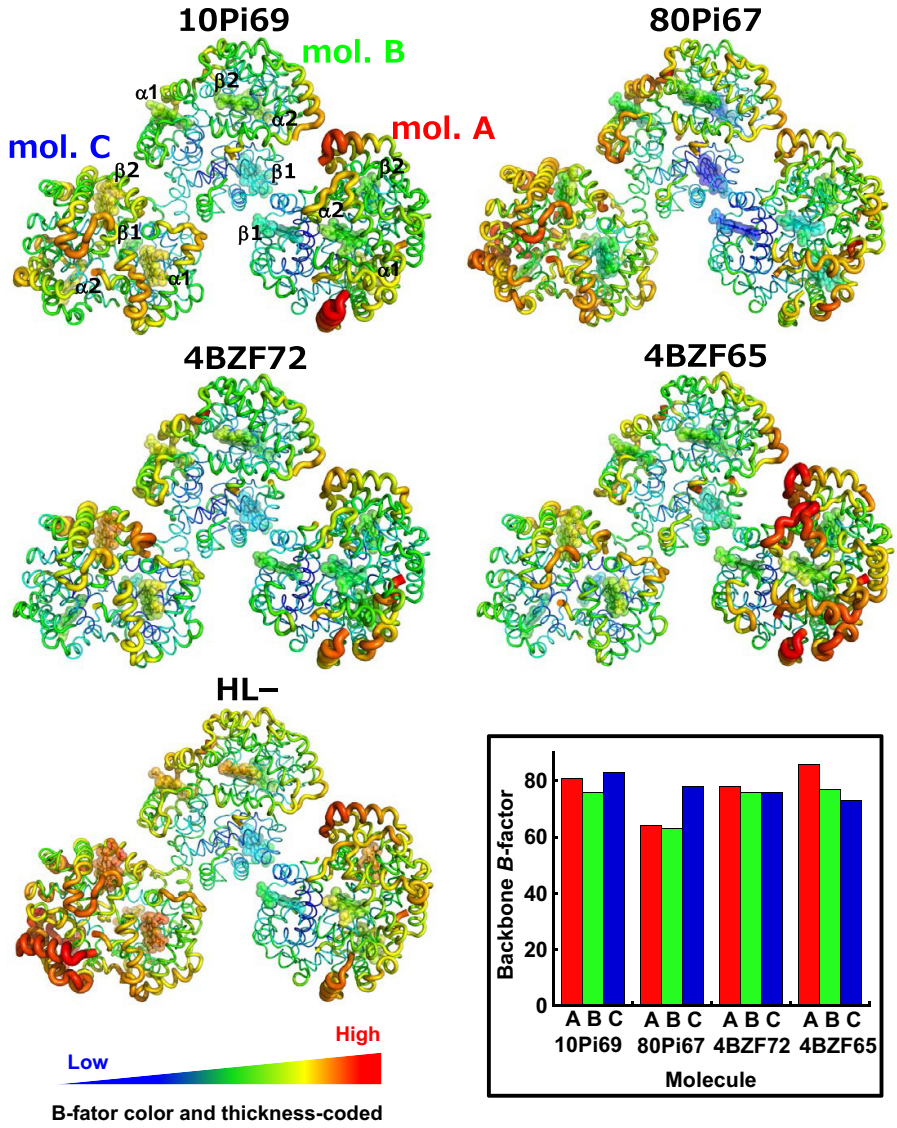


**Figure 8. *B*-factor distributions.** Structures of all Hbs in schematic representation with color and thickness reflecting the scale of the *B*-factors. *Inset* shows comparison of backbone *B*-values (in Å$^2$) averaged over all residues (except residue 1 of each chain) in the 12 tetramers solved in this study.

To date, a number of extended MWC models have been proposed to explain the effector-dependent $O_2$ affinities of the T- and R-states of Hb (9, 34–37). Among them, the tertiary two-state (TTS) model of Henry *et al.* (36, 37) is the simplest possible extension of the MWC model to include pre-existing equilibria of low-affinity and high-affinity tertiary conformations (referred to as *t* and *r*, respectively) in the T or R quaternary conformation. Significantly, this model is consistent with ligand equilibrium data on solutions (38), crystals (20–22), and gels (39), and is also able to fit the kinetic data from CO photodissociation experiments (40). Although the TTS model does not yet make a direct relationship between model parameters and protein structure (37), it predicts that a significant *r* to *t* transition occurs in half-liganded R upon adding strong effectors (*e.g.* IHP or BZF), whereas fully-unliganded T and fully-liganded R contain almost 100% of the subunits in the *t* and *r* conformations, respectively, regardless of solution conditions. However, our data do not indicate that the addition of BZF to half-liganded R induces significant tertiary structural changes (molecules A and B in 4BZF72 and 4BZF65 in Fig. 5*a*), although a modest (5-fold) decrease in affinity was observed (Table 2). Moreover, our previous structural and functional data (13) show the existence of at least three quaternary conformations with different $O_2$ affinities, supporting the quaternary three-state model (9) rather than the TTS model (36, 37).

Interestingly, the addition of $P_i$ or BZF to half-liganded Hb at neutral or acidic pH induces a redistribution of quaternary conformational states, not only along a direction from a relaxed-state to a tense-state but also within relaxed-state populations from R2 to R. Therefore, the R structure represents a critical conformational state connecting both relaxed- and tense-state populations, although the $O_2$ affinity of R is only a few times lower than that of R2 (41). Here we present, based on the present results and our previous report (13), an energy landscape model for half-liganded Hb in the absence and presence of anion or effector (Fig. 9). It is important to note that our present data show that free energy barriers between conformers in our *C*2 crystals are sufficiently low to permit interconversion,

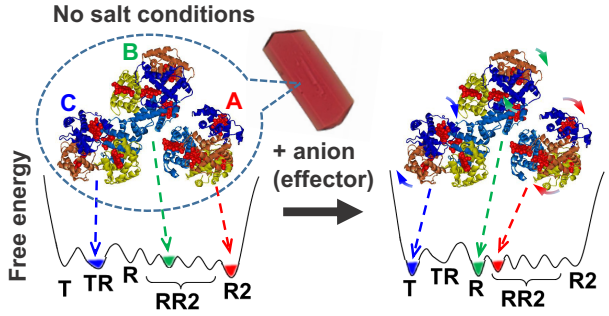


**Figure 9. Schematic showing proposed energy landscape of half-liganded human Hb in the absence (*left*) and presence (*right*) of anion (or effector).**

depending on solution conditions (Fig. 3, *c* and *d*). This allows us to determine unambiguously how effectors can induce conformational changes in Hb, although crystal packing also plays a role in determining the quaternary conformations of the A, B, and C tetramers (*e.g.* the C tetramer favors a T conformation). This will also open up the possibility to perform a time-resolved serial crystallography of the Hb allosteric transition triggered by changing solution conditions of small-sized *C*2 crystals.

The observation of apparently continuous relaxed-state populations in our *C*2 crystals is consistent with recent meta-analysis of hundreds of known crystal structures of human Hb in PDB (7), and also with NMR observation of CO-liganded Hb in solution (8). On the other hand, tense-state populations of Hb appear to be more discrete. In fact, TR is the only conformation that lies between T and R and with an intermediate affinity for $O_2$ (13). No other human Hb structure has ever been captured in the middle of the T to R pathway, despite decades of crystallographic and other studies (11–13, 42–45).

Finally, it is worth noting that sparsely populated states in the conformational ensemble may still play an important role in the regulation of Hb $O_2$ affinity. Considering the $O_2$ affinity difference between conformers (*e.g.* ~25-fold difference between TR and T, as mentioned above), $O_2$ binding does not necessarily take place in the dominant conformer but rather in a less populated conformer that has a greater affinity.

## Experimental procedures

### *Hb preparations and crystallization*

Human adult Hb and XL[$\alpha$(Fe-CO)$\beta$(Ni)][$\alpha$(Ni)$\beta$(Fe-CO)] were prepared and purified as described previously (46). Crystallization was carried out using the microbatch method at 20 °C as described in our previous work (13). Crystals of XL[$\alpha$(Fe-CO)$\beta$(Ni)][$\alpha$(Ni)$\beta$(Fe-CO)] without anions ($HL^-$) were obtained from CO-saturated 1.0% (w/v) XL[$\alpha$(Fe-CO)$\beta$(Ni)][$\alpha$(Ni)$\beta$(Fe-CO)] solution containing 17% (w/v) PEG3350 with no buffer (pH 7.7). To maintain anaerobic conditions during crystallization, the microbatch samples were sealed with CO gas inside a gas-barrier bag including Oxygen Absorbing System A-500HS (ISO, Yokohama, Japan).

### *Microspectrophotometry*

Spectrophotometric measurements on the crystals were carried out at 21–24 °C using a Zeiss UMSP 80 microspectrophotometer. The $HL^-$ crystals were washed with mother liquor containing 25% (w/v) PEG3350 with no buffer (pH 7.7), then immersed and equilibrated with each buffer containing 25% (w/v) PEG3350 and 5% (v/v) glycerol in addition to $P_i$ or BZF. For spectral measurements, a single crystal with 30 $\mu$l of each buffer was placed on a hole-slide glass and then sealed with a coverglass. The absorption spectra of crystals were recorded between 450 and 700 nm with unpolarized light incident on the (010) (or *ac*) crystal face.

Time courses of absorbance changes for thin and thick (2.5–3.0 times thicker) crystals were recorded at 558 and 516 nm, respectively, after transferring the $HL^-$ crystals to each buffer containing 25% (w/v) PEG3350 and 5% (v/v) glycerol in addition to $P_i$ or BZF. Time zero is defined as the time when the $HL^-$ crystal was immersed in a buffer containing $P_i$ or BZF. The dead time of these kinetic experiments, from addition of an effector to initiation of data collection, is 30–40 s.

### *Conformational population shifts induced by changing in solution conditions*

The conformational ensembles under four solution conditions were determined by X-ray crystallography after soaking the $HL^-$ crystals in each buffer containing 25% (w/v) PEG3350 and 5% (v/v) glycerol for a sufficient time period. The buffer conditions studied are as follows: 10 mM $P_i$-K buffer (pH 6.9) (10Pi69), 80 mM $P_i$-K buffer (pH 6.7) (80Pi67), 4 mM BZF and 20 mM HEPES buffer (pH 7.2) (4BZF72), and 4 mM BZF and 20 mM MES buffer (pH 6.5) (4BZF65). For all the crystals, the buffers containing 15% (v/v) glycerol were used as cryoprotectant in which the crystals were rinsed briefly before flash-freezing in liquid nitrogen. Note here that the increase in concentration of glycerol from 5 to 15% does not so much affect the conformational ensembles of half-liganded Hb, as judged from the similarity of the absorption spectra of crystals with 5 and 15% glycerol. A previous study also indicated that 75% (v/v) glycerol does not significantly affect the points of the T and R equilibration in CO-bound carp Hb in the absence and presence of IHP (47).

### *Data collection and structure determination*

X-ray data were collected using the synchrotron radiation source at the beam line AR-NW12A station of the Photon Factory, Tsukuba, Japan, using an ADSC Quantum 315 CCD detector. All data were processed and scaled using HKL2000 and SCALEPACK (48). All the crystals were of the same *C*2 space group with comparable cell parameters. All the structures were solved by molecular replacement using PHASER (49). To minimize the model bias on the quaternary structure, the $\alpha\beta$ dimer (not the tetramer) of human oxy-Hb (50) (PDB code 2DN1) was used as the initial search model. The orientations and positions of the three tetramer Hb molecules in the asymmetric unit were initially optimized by rigid-body refinement against data between 20- and 3-Å resolution. The models were further refined using the Translation-Libration-Screw method (51) to assign an anisotropic motion to each protein subunit. The data resolution limits were 20.0–2.70 Å (10Pi69), 20.0–2.53 Å (80Pi67), and 20.0–2.65 Å resolution (4BZF72) or 20.0–2.40-Å resolution (4BZF65). The electron density was interpreted and traced using COOT (52) and the model was refined

with PHENIX (53) and autoBUSTER (54). Structural evaluation of the final models of Hbs using MolProbity (55) indicated that ~95% of the residues are in the most favorable regions of the Ramachandran plot. Details of data collection and structure refinement are given in Table 1.

### *Difference distance matrices*

Difference distance matrices of the ($\alpha1\beta1$)($\alpha2\beta2$) subunits of each tetramer were calculated using an appropriate reference structure by the program DDMP (Center for Structural Biology, Yale University, New Haven, CT).

### *Overlap method*

The least-squares superpositions of different models were made using an in-house program CFIT.[3] The C$\alpha$ atoms of all residues except the N-terminal residue were used, so that 570 atoms were matched in each tetramer overlay. To find the dimer–dimer rotation angle, $\alpha\beta$ dimer pairs were fitted sequentially.

### *$O_2$ equilibrium measurement*

The $O_2$ equilibrium curves of crystals were determined as described (13, 41). Crystals of 10Pi69, 80Pi67, 4BZF72, and 4BZF65 were prepared by soaking the $HL^-$ crystals in each buffer containing 25% (w/v) PEG3350 and 0.1 mg/ml of catalase (Sigma) with no glycerol added. A single crystal with about 10 $\mu$l of its mother liquor was placed on a coverglass and then sealed in a flow chamber mounted on the stage of a Zeiss UMSP 80 microspectrophotometer. Before measurements, removal of CO was carried out in the flow chamber with humidified $O_2$, at a gas flow of 10 ml/min, under illumination with white light. Humidified $N_2/O_2$ gas mixtures at defined partial $O_2$ pressures were prepared by a GB-4C gas blender (Kofloc, Japan) with modifications, and flowed into the chamber at a gas flow of 10 ml/min. The $O_2$ pressures were detected in the outflow from the chamber using a MC-7G-L galvanic $O_2$ sensor (Iijima, Japan). The absorption spectra of crystals equilibrated with different $O_2$ pressures at 21–23 °C were recorded between 450 and 700 nm with unpolarized light incident on (010) crystal face. According to the method of Mozzarelli *et al.* (20, 21), the fractional saturation of the ferrous hemes with $O_2$ was calculated by a least-square fit of the observed absorption spectra to a linear combination of three reference spectra and a baseline offset. The reference spectra are the absorption spectra of crystals of oxy-, deoxy-, and met-forms of each Hb sample. Because full $O_2$ saturation could not be attained for these crystals even under $O_2$ atmosphere, the data at the highest pressures were extrapolated to infinite $O_2$ pressure to obtain the oxy-form spectra. After each $O_2$ equilibrium measurement, the crystal was reduced by washing with mother liquor containing 0.05% (w/v) sodium dithionite for the measurement of the deoxy-form reference spectrum. The crystal was then washed with mother liquor to remove sodium dithionite, followed by washing with mother liquor containing 5 mM potassium ferricyanide to oxidize the crystal for the measurement of the met-form reference spectrum.

[3] J. R. H. Tame, unpublished data.

### *Determination of $O_2$ affinity*

According to the biphasic model (see "Results and discussion"), $O_2$ dissociation curves were fitted using the equation: $Y(p) = (1\text{-}C)Y_{AB}(p) + CY_C(p)$, where $p$ is the partial $O_2$ pressure, $C$ is the relative spectral contribution of molecule C (low-affinity component) to the total absorption, $Y_{AB}(p)$ is the fractional saturation of the sum of molecule A and B (high-affinity component), and $Y_C(p)$ is the fractional saturation of molecule C. The model assumes that the first and second $O_2$ association equilibrium constants, $K_1$ and $K_2$, of molecules C in all the current crystals (Fe(II)-Ni(II) hybrid contains two Fe(II)-hemes per tetramer; see Fig. 1*b*) are the same as those of the $HL^+$ crystal previously determined (13), and thus $Y_C(p)$ is defined as,

$$Y_C(p) = \frac{K_{1C}p + K_{1C}K_{2C}p^2}{1 + 2K_{1C}p + K_{1C}K_{2C}p^2} \quad \text{(Eq. 1)}$$

where the two equilibrium constants are fixed to be $K_{1C} = 0.0132$ torr$^{-1}$ and $K_{2C} = 0.00646$ torr$^{-1}$. Note that this $K_{2C}$ value represents the $O_2$ affinity of molecules C in all the current crystal structures (Table 2). The model also assumes that $Y_{AB}(p)$ can be approximately described by two $O_2$ binding constants $K_{1AB}$ and $K_{2AB}$, and thus $Y_{AB}(p)$ is in the same form as $Y_C(p)$ and is defined as,

$$Y_{AB}(p) = \frac{K_{1AB}p + K_{1AB}K_{2AB}p^2}{1 + 2K_{1AB}p + K_{1AB}K_{2AB}p^2} \quad \text{(Eq. 2)}$$

where $K_{2AB}$ represents the overall $O_2$ affinity of molecules A and B in the current crystal structures, and the Hill coefficient at half-saturation ($n$), a measure of cooperativity, can be calculated from $K_{1AB}$ and $K_{2AB}$ by using the following formula.

$$n = \frac{2}{1 + \sqrt{\frac{K_{1AB}}{K_{2AB}}}} \quad \text{(Eq. 3)}$$

*Author contributions*—N. S. conceived and coordinated this study, prepared and crystallized the Hb sample, performed microspectrophotometry and $O_2$ equilibrium measurements, and wrote the manuscript. All authors collected and analyzed X-ray data, contributed to constructing the manuscript, and approved the final version of the manuscript.

**References**


1. Monod, J., Wyman, J., and Changeux, J.-P. (1965) On the nature of allosteric transitions: a plausible model. *J. Mol. Biol.* **12,** 88–118
2. Baldwin, J., and Chothia, C. (1979) Haemoglobin: the structural changes related to ligand binding and its allosteric mechanism. *J. Mol. Biol.* **129,** 175–220
3. Perutz, M. F. (1989) Mechanisms of cooperativity and allosteric regulation in proteins. *Q. Rev. Biophys.* **22,** 139–237
4. Silva, M. M., Rogers, P. H., and Arnone, A. (1992) A third quaternary structure of human hemoglobin A at 1.7-Å resolution. *J. Biol. Chem.* **267,** 17248–17256
5. Biswal, B. K., and Vijayan, M. (2001) Structure of human methaemoglobin: the variation of a theme. *Curr. Sci.* **81,** 1100–1105
6. Safo, M. K., and Abraham, D. J. (2005) The enigma of the liganded hemoglobin end state: a novel quaternary structure of human carbonmonoxy hemoglobin. *Biochemistry* **44,** 8347–8359

7. Ren, Z. (2013) Reaction trajectory revealed by a joint analysis of protein data bank. *PLoS ONE* **8,** e77141
8. Lukin, J. A., Kontaxis, G., Simplaceanu, V., Yuan, Y., Bax, A., and Ho, C. (2003) Quaternary structure of hemoglobin in solution. *Proc. Natl. Acad. Sci. U.S.A.* **100,** 517–520
9. Minton, A. P., and Imai, K. (1974) The three-state model: a minimal allosteric description of homotropic and heterotropic effects in the binding of ligands to hemoglobin. *Proc. Natl. Acad. Sci. U.S.A.* **71,** 1418–1421
10. Schumacher, M. A., Dixon, M. M., Kluger, R., Jones, R. T., and Brennan, R. G. (1995) Allosteric transition intermediates modeled by cross-linked haemoglobins. *Nature* **375,** 84–87
11. Colombo, M. F., and Seixas, F. A. (1999) Novel allosteric conformation of human HB revealed by the hydration and anion effects on $O_2$ binding. *Biochemistry* **38,** 11741–11748
12. Shibayama, N., and Saigo, S. (2001) Direct observation of two distinct affinity conformations in the T state human deoxyhemoglobin. *FEBS Lett.* **492,** 50–53
13. Shibayama, N., Sugiyama, K., Tame, J. R., and Park, S. Y. (2014) Capturing the hemoglobin allosteric transition in a single crystal form. *J. Am. Chem. Soc.* **136,** 5097–5105
14. Shibayama, N. (1999) Functional analysis of hemoglobin molecules locked in doubly liganded conformations. *J. Mol. Biol.* **285,** 1383–1388
15. Shibayama, N., Morimoto, H., and Miyazaki, G. (1986) Oxygen equilibrium study and light absorption spectra of Ni(II)-Fe(II) hybrid hemoglobins. *J. Mol. Biol.* **192,** 323–329
16. Shibayama, N., Morimoto, H., and Kitagawa, T. (1986) Properties of chemically modified Ni(II)-Fe(II) hybrid hemoglobins: Ni(II) protoporphyrin IX as a model for a permanent deoxy-heme. *J. Mol. Biol.* **192,** 331–336
17. Shibayama, N., Imai, K., Hirata, H., Hiraiwa, H., Morimoto, H., and Saigo, S. (1991) Oxygen equilibrium properties of highly purified human adult hemoglobin cross-linked between 82$\beta$1 and 82$\beta$2 lysyl residues by bis(3,5-dibromosalicyl)fumarate. *Biochemistry* **30,** 8158–8165
18. Park, S.-Y., Shibayama, N., Hiraki, T., and Tame, J. R. (2004) Crystal structures of unliganded and half-liganded human hemoglobin derivatives cross-linked between Lys82$\beta$1 and Lys82$\beta$2. *Biochemistry* **43,** 8711–8717
19. Perutz, M. F., Fermi, G., Abraham, D. J., Poyart, C., and Bursaux, E. (1986) Hemoglobin as a receptor of drugs and peptides: x-ray studies of the stereochemistry of binding. *J. Am. Chem. Soc.* **108,** 1064–1078
20. Mozzarelli, A., Rivetti, C., Rossi, G. L., Henry, E. R., and Eaton, W. A. (1991) Crystals of haemoglobin with the T quaternary structure bind oxygen noncooperatively with no Bohr effect. *Nature* **351,** 416–419
21. Rivetti, C., Mozzarelli, A., Rossi, G. L., Henry, E. R., and Eaton, W. A. (1993) Oxygen binding by crystals of hemoglobin. *Biochemistry* **32,** 2888–2906
22. Mozzarelli, A., Rivetti, C., Rossi, G. L., Eaton, W. A., and Henry, E. R. (1997) Allosteric effectors do not alter the oxygen affinity of hemoglobin crystals. *Protein Sci.* **6,** 484–489
23. Imai, K. (1979) Thermodynamic aspects of the co-operativity in four-step oxygenation equilibria of haemoglobin. *J. Mol. Biol.* **133,** 233–247
24. Perutz, M. F. (1968) Preparation of haemoglobin crystals. *J. Crystal Growth* **2,** 54–56
25. Shaanan, B. (1983) Structure of human oxyhaemoglobin at 2.1-Å resolution. *J. Mol. Biol.* **171,** 31–59
26. Derewenda, Z., Dodson, G., Emsley, P., Harris, D., Nagai, K., Perutz, M., Renaud, J. P., and Reynaud, J.-P. (1990) Stereochemistry of carbon monoxide binding to normal human adult and Cowtown haemoglobins. *J. Mol. Biol.* **211,** 515–519
27. Sen, U., Dasgupta, J., Choudhury, D., Datta, P., Chakrabarti, A., Chakrabarty, S. B., Chakrabarty, A., and Dattagupta, J. K. (2004) Crystal structures of $HbA_2$ and HbE and modeling of hemoglobin $\delta_4$: interpretation of the thermal stability and the antisickling effect of $HbA_2$ and identification of the ferrocyanide binding site in Hb. *Biochemistry* **43,** 12477–12488
28. Patskovska, L. N., Patskovsky, Y. V., Almo, S. C., and Hirsch, R. E. (2005) COHbC and COHbS crystallize in the R2 quaternary state at neutral pH in the presence of PEG 4000. *Acta Crystallogr. D Biol. Crystallogr.* **61,** 566–573
29. Ringe, D., and Petsko, G. A. (1986) Study of protein dynamics by X-ray diffraction. *Methods Enzymol.* **131,** 389–433
30. Mehanna, A. S., and Abraham, D. J. (1990) Comparison of crystal and solution hemoglobin binding of selected antigelling agents and allosteric modifiers. *Biochemistry* **29,** 3944–3952
31. Koshland, D. E., Jr., Némethy, G., and Filmer, D. (1966) Comparison of experimental binding data and theoretical models in proteins containing subunits. *Biochemistry* **5,** 365–385
32. Gunasekaran, K., Ma, B., and Nussinov, R. (2004) Is allostery an intrinsic property of all dynamic proteins? *Proteins* **57,** 433–443
33. Boehr, D. D., Nussinov, R., and Wright, P. E. (2009) The role of dynamic conformational ensembles in biomolecular recognition. *Nat. Chem. Biol.* **5,** 789–796
34. Szabo, A., and Karplus, M. (1972) A mathematical model for structure function relations in hemoglobin. *J. Mol. Biol.* **72,** 163–197
35. Lee, A. W., and Karplus, M. (1983) Structure-specific model of hemoglobin cooperativity. *Proc. Natl. Acad. Sci. U.S.A.* **80,** 7055–7059
36. Henry, E. R., Bettati, S., Hofrichter, J., and Eaton, W. A. (2002) A tertiary two-state allosteric model for hemoglobin. *Biophys. Chem.* **98,** 149–164
37. Henry, E. R., Mozzarelli, A., Viappiani, C., Abbruzzetti, S., Bettati, S., Ronda, L., Bruno, S., and Eaton, W. A. (2015) Experiments on hemoglobin in single crystals and silica gels distinguish among allosteric models. *Biophys. J.* **109,** 1264–1272
38. Perrella, M., Colosimo, A., Benazzi, L., Ripamonti, M., and Rossi-Bernardi, L. (1990) What the intermediate compounds in ligand binding to hemoglobin tell about the mechanism of cooperativity. *Biophys. Chem.* **37,** 211–223
39. Bruno, S., Bonaccio, M., Bettati, S., Rivetti, C., Viappiani, C., Abbruzzetti, S., and Mozzarelli, A. (2001) High and low oxygen affinity conformations of T state hemoglobin. *Protein Sci.* **10,** 2401–2407
40. Jones, C. M., Ansari, A., Henry, E. R., Christoph, G. W., Hofrichter, J., and Eaton, W. A. (1992) The speed of intersubunit communication in proteins. *Biochemistry* **31,** 6692–6702
41. Shibayama, N., Sugiyama, K., and Park, S.-Y. (2011) Structures and oxygen affinities of crystalline human hemoglobin C ($\beta$6 Glu→Lys) in the R and R2 quaternary structures. *J. Biol. Chem.* **286,** 33661–33668
42. Arnone, A., Rogers P, Blough, N. V., McGourty, J. L., and Hoffman, B. M. (1986) X-ray diffraction studies of a partially liganded hemoglobin, $[\alpha(\text{FeII-CO})\beta(\text{MnII})]_2$. *J. Mol. Biol.* **188,** 693–706
43. Luisi, B., and Shibayama, N. (1989) Structure of haemoglobin in the deoxy quaternary state with ligand bound at the $\alpha$ haems. *J. Mol. Biol.* **206,** 723–736
44. Luisi, B., Liddington, B., Fermi, G., and Shibayama, N. (1990) Structure of deoxy-quaternary haemoglobin with liganded $\beta$ subunits. *J. Mol. Biol.* **214,** 7–14
45. Seixas, F. A., de Azevedo, W. F., Jr., and Colombo, M. F. (1999) Crystallization and x-ray diffraction data analysis of human deoxyhaemoglobin $A_0$ fully stripped of any anions. *Acta Crystallogr. D Biol. Crystallogr.* **55,** 1914–1916
46. Shibayama, N., Imai, K., Morimoto, H., and Saigo, S. (1995) Oxygen equilibrium properties of nickel(II)-iron(II) hybrid hemoglobins cross-linked between 82$\beta$1 and 82$\beta$2 lysyl residues by bis(3,5-dibromosalicyl)fumarate: determination of the first two-step microscopic Adair constants for human hemoglobin. *Biochemistry* **34,** 4773–4780
47. Cobau, W. G., LeGrange, J. D., and Austin, R. H. (1985) Kinetic differences at low temperatures between R and T state carbon monoxide-carp hemoglobin. *Biophys. J.* **47,** 781–786
48. Otwinowski, Z., and Minor, W. (1997) Processing of X-ray diffraction data collected in oscillation mode. *Methods Enzymol.* **276,** 307–326
49. McCoy, A. J., Grosse-Kunstleve, R. W., Adams, P. D., Winn, M. D., Storoni, L. C., and Read, R. J. (2007) Phaser crystallographic software. *J. Appl. Crystallogr.* **40,** 658–674
50. Park, S. Y., Yokoyama, T., Shibayama, N., Shiro, Y., and Tame, J. R. (2006) 1.25 Å resolution crystal structures of human haemoglobin in the oxy, deoxy and carbonmonoxy forms. *J. Mol. Biol.* **360,** 690–701
51. Winn, M. D., Isupov, M. N., and Murshudov, G. N. (2001) Use of TLS parameters to model anisotropic displacements in macromolecular refinement. *Acta Crystallogr. D Biol. Crystallogr.* **57,** 122–133

52. Emsley, P., Lohkamp, B., Scott, W. G., and Cowtan, K. (2010) Features and development of Coot. *Acta Crystallogr. D Biol. Crystallogr.* **66,** 486–501
53. Adams, P. D., Afonine, P. V., Bunkóczi, G., Chen, V. B., Davis, I. W., Echols, N., Headd, J. J., Hung, L.-W., Kapral, G. J., Grosse-Kunstleve, R. W., McCoy, A. J., Moriarty, N. W., Oeffner, R., Read, R. J., Richardson, D. C., *et al*. (2010) PHENIX: a comprehensive Python-based system for macromolecular structure solution. *Acta Crystallogr. D Biol. Crystallogr.* **66,** 213–221
54. Bricogne, G., Blanc, E., Brandl, M., Flensburg, C., Keller, P., Paciorek, W., Roversi, P., Sharff, A., Smart, O. S., Vonrhein, C., and Womack, T. O. (2011) *BUSTER version 2.10.2.* Global Phasing Ltd., Cambridge, United Kingdom
55. Chen, V. B., Arendall, W. B 3rd, Headd, J. J., Keedy, D. A., Immormino, R. M., Kapral, G. J., Murray, L. W., Richardson, J. S., and Richardson, D. C. (2010) MolProbity: all-atom structure validation for macromolecular crystallography. *Acta Crystallogr. D Biol. Crystallogr.* **66,** 12–21
56. Shibayama, N. (2011) in *Hemoglobin: Recent Developments and Topics* (Nagai, M., ed) pp. 138–140, Research Signpost, Kerala